Mongolian Journal of Chemistry
www.mongoliajol.info/index.php/MJC

Monte Carlo and DFT calculations on the corrosion inhibition efficiency of some benzimide molecules

Dyari Mustafa Mamand[1], Yousif Hussein Azeez[2], Hiwa Mohammad Qadr[1*]

[1]*University of Raparin, College of Science, Department of Physics, Sulaymaniyah, 46012, Iraq*
[2]*Halabja University, College of Science, Department of Physics, Halabja, 46018, Iraq*

** Corresponding author: hiwa.physics@uor.edu.krd;* ORCID ID: 0000-0001-5585-3260

Received: 1 December 2022; revised: 23 April 2023; accepted: 25 April 2023

ABSTRACT

Calculations using density functional theory (DFT) and Monte Carlo methods were performed on 2-methylbenzimidazole, 2-mercaptobenzimidazole, 2-aminobenzimidazole, benzotriazole, and benzimidazole to determine their corrosion inhibition efficiency. The molecular structure was optimized geometrically using DFT calculations at the B3LYP/6–311 G++(d,p) and b2plypd3/aug-cc-pvdz basis set level in protonated and non-protonated species in gas and water. In this study, HOMO, LUMO, bandgap, ionization energy, electronegativity, hardness, softness, electrophilicity and nucleophilicity, electron transfer, back donation energy and condensed Fukui indices are used to assess a molecule's local reactivity. Theoretical investigations can precisely establish the geometrical dimensions of a molecule and correctly explain the quantum properties of inhibitors. The mechanism of interaction between inhibitors and metal surfaces in a specified molecule is studied using molecular dynamics. The benzimidazole functional groups absorbed energy linearly on metal surfaces, with quantum characteristics determined using density functional theory and an ab initio technique. Importantly, the findings of this conceptual model are consistent with the corrosion inhibition efficiency of earlier experimental investigations.

Keywords: DFT, Monte Carlo, benzimide, corrosion

INTRODUCTION

The oxide layer in metals causes structural deterioration. Corrosion conditions, such as hydrochloric acid and nitric acid, typically activate this reaction [1, 2]. Corrosion is a complex process to overcome, and if left uncontrolled, it can cause high economic losses. As a result, considerable research is already being conducted to identify corrosion inhibitors that are ecologically benign, inexpensive, and efficient [3, 4]. Natural organic molecules have a strong potential for development as corrosion inhibitors. This molecule was chosen as a corrosion inhibitor because it fits the requirements of high efficiency, low cost, environmental friendliness, non-toxicity, and no hazardous pollutants. Several experimental studies on the corrosion inhibition efficacy of organic product molecules have been conducted. Alkaloids derived from natural products, for instance, have great potential as corrosion inhibitors. The main mechanisms that limit corrosion are related to electron acceptors, electrostatic interactions, electron donors, and heteroatom groups on inhibitor molecules. In the alkaloid structure, heterocyclic benzene and heteroatom groups such as Nitrogen, Sulphur, Oxygen and heteroatoms perform roles as electron donors, electrostatic interactions, and the metal surface interactions with electron donor acceptors. The inhibitor will use these characteristics to get securely adhered to the metal surface and build a thin coating that will prevent the pace of corrosion.

2-Methylbenzimidazole is a significant pharmacophore that is frequently utilized in biomedical sciences to synthesize a variety of antibacterial and antifungal drugs. It can serve as a crucial precursor in the synthesis of substituted benzimidazole [5, 6]. 2-mercaptobenzimidazole is frequently utilized as a rubber accelerator and as an antioxidant for rubber and plastics. 2-Mercaptobenzimidazole and its products are insecticides, and it is also a prominent analytical reagent for mercury, had been used to determine Cd(II), Cu(II) and Fe(II) metal ions in industrial wastewater samples and sewage water [7-9]. As antibiofilm agents, 2-aminobenzimidazole and its derivatives have been produced. Several studies have shown that 2-aminobenzimidazole may selectively suppress and

disperse Gram-positive and Gram-negative bacterial biofilms without affecting free germ cell growth. A no microbicidal chemical that affects biofilm formation may be used as an additional ingredient in an antibiofilm approach. Because even if a chemical efficiently suppresses biofilm formation without killing the microbial cells, planktonic cells can attach to other sites and form a biofilm. As a result, 2-aminobenzimidazole derivatives and antibiotics are effective against bacterial biofilms [10]. Benzimidazole and its derivatives are recognized as a major heterocyclic motif with several pharmacological uses, especially anti-diabetics, anti-cancer, anti-convulsant, antivirals, antifungals, anti-hypertensives and anti-HIVs [11]. Because of its anti-mycobacterial characteristics, benzotriazole is appealing as a heterocycle [12]. Corrosion inhibitors are among the most extensively used and cost-effective techniques for preventing corrosion in metals and alloys. Typical corrosion inhibitors are bio-toxic chemical substances with substantial toxicity problems. Drugs are mostly used as corrosion inhibitors. The use of pharmaceuticals as corrosion inhibitors of metal corrosion has some advantages over the use of various inorganic/organic inhibitors due to their low or negligible impact on the environment. Because the drugs are harmless, inexpensive, and have minor environmental consequences, it is best to replace the current corrosion-damaging inhibitor. Many of those skilled in the art feel that the drugs are corrosion inhibitors that can compare favorably with identified green rust inhibitors and that most of these drugs, cabe synthesized from natural compounds.

In this study, great attention has been paid to the electronic structure and chemical properties of each inhibitor shown in Fig. 1: 2-methylbenzimidazole, 2-mercapto benzimidazole, 2-aminobenzimidazole, benzotriazole and benzimidazole. Through their use, we were able to reach a conclusion that is consistent with previous experimental results regarding their ability to prevent corrosion.

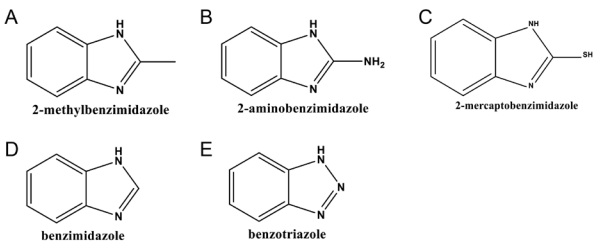

Fig. 1. Chemical structures of all inhibitors.

Computational detail: The quantum chemical calculations have been carried out at DFT (B3LYP) methods with 6-311++G (d, p) and b2plypd3/aug-cc-pvdz with Gaussian09 software [13, 14]. Because electrochemical corrosion occurs in the liquid phase, including the influence of solvent is computationally feasible. The calculations in the solution were carried out using the self-consistent reaction field (SCRF) concept and Tomasi's polarized continuum model (PCM) [15]. These approaches describe the cavity in which the solute is inserted as a uniform sequence of interconnecting atomic spheres and model the solution as a continuum of uniform dielectric constant (DC= 78.5). As well as, the Fukui functions and the thermodynamic parameters were tabulated. Kinetic stability and chemical reactivity properties of the optimized molecular structure have been found by the frontier molecular orbitals (FMOs).

RESULTS AND DISCUSSIONS

DFT with Global Chemical Reactivity Descriptors: The global reactivity indices provide information on a chemical compound's stability, reactivity, and selectivity. Global reactivity characteristics such as energy gap (E_g), global hardness (η), global softness (S), electronegativity (χ), chemical potential (μ), maximal amount of electronic charge (Q^{max}), electrophilicity (ω), electrodonating power (ω^-), electroaccepting power (ω^+), and net electrophilicity based on DFT with 6311++G (d,p) and b2plypd3/aug-cc-pvdz were calculated by using the energies of the frontier orbitals and Gaussian 09 software (1-10) [16-19].

$$IP = -E_{HOMO} \quad \text{and} \quad EA = -E_{LUMO} \tag{1}$$

$$E_g = E_{LUMO} - E_{HOMO} \tag{2}$$

$$\chi = \frac{E_{HOMO} + E_{LUMO}}{2} \tag{3}$$

$$\mu = -\frac{(E_{HOMO} + E_{LUMO})}{2} \tag{4}$$

$$\eta = \frac{E_{LUMO} - E_{HOMO}}{2} \tag{5}$$

$$S = \frac{1}{2\eta} \tag{6}$$

$$\omega = \frac{\mu^2}{2\eta} \tag{7}$$

$$\Delta N = \frac{\chi_{cu} - \chi_{inh}}{2\sum \eta_{cu} - \eta_{inh}} \tag{8}$$

$$\varepsilon = \frac{1}{\omega} \tag{9}$$

$$\Delta E_{back-donation} = \frac{-\eta}{4} \tag{10}$$

Fukui Function (local reactivity descriptors): The Fukui Function gives information on the reactivity indices in a given system. For the highest Fukui function values, the atom exhibits a significant degree of reactivity. The Fukui functions from (compound 1-5) has been calculated on the basis of B3LYP/6–311++G(d,p) and b2plypd3/aug-cc-pvdz level of theory, and the results are shown in Tables 1-4. The Fukui Functions (f^-_k, f^+_k) are computed using mulliken population analysis charges of negative and positive ions and are given in Tables 7, 9, 11, and 13 using

equations 11 and 12. If (N) represents the number of electrons, then (N + 1) denotes an ion and (N – 1) denotes the system's cation [20].

$$f_k^+ = q(N+1) - q(N) \quad (11)$$

$$f_k^- = q(N) - q(N-1) \quad (12)$$

Quantum chemical parameters: Quantum chemical calculations have long been used to study reaction processes. They have very effective tools for studying metal corrosion inhibition [21, 22]. The electrostatics and spatial molecules of a corrosion inhibition efficiency are directly related to its performance, the relationships between quantum chemical properties and inhibitory effect studied in this work. The calculation of quantum chemical parameters in corrosion inhibition investigations includes two basic characteristics: first, identifying the correlation between inhibitor molecular structure and inhibitory behavior; and second, developing a hypothesized inhibition mechanism in terms of chemical reactivity of compounds [23]. In addition, quantum chemical descriptor variables were related to experimental values to explore inhibitor molecular reactivity. The frontier molecular orbitals (E_{HOMO}, E_{LUMO}) and quantum chemical indices such as molecular hardness, molecular softness, electronegativity, and chemical potential are tabulated in Tables 1-4. Interaction between reacting species occurs through FMOs (E_{HOMO} and E_{LUMO}). Furthermore, ionization potential (IP) = E_{HOMO} relates to the capacity of the inhibitor to donate electrons and indicates the electron-donating propensity of the molecule. Thus, higher value of E_{HOMO} signifies better propensity of donating electron, and enhancing the adsorption of the inhibitor on the metal surface and so better inhibition performance. E_{LUMO} energy is connected to electron affinity (EA) = E_{LUMO} and shows the ability of a molecule to receive electrons. Thus, better capacity to receive electrons is indicated by a lower value of E_{LUMO}, which will also improve the adsorption of the inhibitor on the metal surface and therefore improve inhibition effectiveness [24]. As can be seen in Tables 1 and 3, the greatest value of E_{HUMO} and the lowest value of E_{LUMO} for the caffeine compound compared to other findings in gas phase and solvent phase (water) show that 2-methylbenzimidazol has a higher inhibitory efficiency, which is consistent with the experimental result.

The ionization energy of an element is the ability of materials to participate in chemical processes that require ion creation or electron donation. It is also often connected to the type of chemical bonding in the elements' complexes [25]. The ionization potential of an inhibitor can be used to determine its reactivity. As displayed in Tables 1-4, a high ionization potential value implies that the compound is very reactive, whereas a low ionization potential value suggests that the molecule is inactive. 2-amino benzimidazole has the highest corrosion inhibition efficiency.

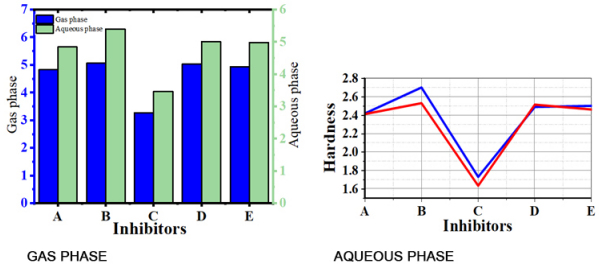

Fig. 2. Bandgap and harness of selected inhibitors in gas and aqueous phase.

The frontier energy gap between E_{HOMO} and E_{LUMO} is an essential characteristic for inhibitor molecule adsorption on metallic surfaces. Lower energy differences improve inhibition efficiency and reactivity, because it takes less energy to remove an electron from the last occupied orbital. The 2-methylbenzimidazol inhibitor has the smallest energy gap compared to other compounds, as shown in Fig. 2 and Tables 1 and 4. This suggests that the 2-mercaptobenzimidazol molecule may have superior performance compared to the other molecule, a conclusion that is consistent with the experimental result. The global hardness and softness are significant for evaluating the stability and reactivity of molecules. Hard molecules have big energy gaps whereas soft molecules have small ones [26]. Our results in Tables 1, 3 and Fig. 2, A and B reveals that, 2-mercapto benzimidazole and 2-methylbenzimidazol has low hardness than the rest of molecules in gas phase and solvent phase. The inhibitor with the lowest absolute hardness value is predicted to be the most effective in inhibiting a target molecule. 2-methylbenzimidazol and benzotriazole have a greater softness than other compounds in gas and solvent medium.

Electronegativity (χ) is another characteristic of inhibitory efficiency, and electronegativity values found for the evaluated inhibitor molecules may offer information about the covalent interactions between the inhibitor and the metal surface [27, 28]. According to the data in Tables 1-4, 2-mercaptobenzimidazole and 2-methylbenzimidazol has the lowest absolute electronegativity (maximum chemical potential). 2-mercaptobenzimidazole and 2-methylbenzimidazol has a higher inhibitory effectiveness due to its low electronegativity and high chemical potential. 2-aminobenzimidazole has the lowest corrosion inhibition efficiency compare with all other inhibitors in this study. Nucleophilicity and electrophilicity are plausible quantum chemical variables for predicting molecule chemical behavior. These values can be used to evaluate inhibitor performance [27]. It should be mentioned that a compound with a high electrophilicity value is useless for corrosion inhibition. In contrast, 2-mercaptobenzimidazol, which has a high nucleophilicity value, is an excellent corrosion inhibitor [28].

When Fe and inhibitor are combined, electrons flow from inhibitor to Fe until the chemical potential is equal. The fraction of electrons transferred ΔN, computed by considering the absolute electronegativity of iron (X_{Fe}=7 eV) and global hardness (η_{Fe}=0), assuming metallic bulk IP =EA [29]. When ΔN is less than 3.6, the capacity of the compounds (inhibitors) to donate electrons to the metal surface increases the inhibition efficiency. In our investigation, inhibition efficiency also increased as ΔN values increased [30].

Therefore, the highest fraction of transferred electrons is related with the most effective inhibitor (2-mercaptobenzimidazole), whereas the lowest fraction is associated with the least effective inhibitor (2-aminobenzimidazole).

Tables 1 to 4 also includes the computed $E_{Back\text{-}donation}$ values for the all the compounds (inhibitors) in gas phase and in water solvent. The reverse donation of charges is the negative of hardness (-η/4) in the presence of charge transfer, which governs the interaction between

Table 1. Quantum chemical parameters in gas phase at B3LYP/6–311 G++(d,p).

Indices	2-amino benzimidazole	2-methyl benzimidazol	2-mercapto benzimidazole	benzimidazole	benzotriazole
E_{HOMO} (eV)	-5.842	-5.369	-5.91	-5.461	-6.282
E_{LUMO} (eV)	-0.781	-0.544	-0.639	-0.536	-1.252
IP (eV)	5.842	5.369	3.91	5.461	6.282
EA (eV)	0.781	0.544	0.639	0.536	1.252
Eg (eV)	5.061	4.825	3.271	4.925	5.03
η(eV)	2.531	2.413	1.6355	2.4625	2.515
S $(eV)^{-1}$	0.198	0.207	0.611434	0.406091	0.397614
χ(eV)	3.312	2.957	2.2745	2.9985	3.767
μ (eV)	-3.312	-2.957	-2.2745	-2.9985	-3.767
ω (eV)	2.167	1.812	1.581581	1.825584	2.821131
$ε(eV)^{-1}$	0.461	0.552	0.632279	0.54777	0.354468
ΔN	0.330	0.419	1.444665	0.812487	0.642744
$ΔE_{(back\text{-}donation)}$(eV)	-0.63275	-0.60325	-0.40888	-0.61563	-0.62875

Table 2. Quantum chemical parameters in gas phase at b2plypd3/aug-cc-pvdz.

Indices	2-amino benzimidazole	2-methyl benzimidazol	2-mercapto benzimidazole	benzimidazole	benzotriazole
E_{HOMO} (eV)	-6.241	-7.047	-6.627	-7.231	-7.789
E_{LUMO} (eV)	-1.678	-2.516	-3.203	-0.602	-0.126
IP (eV)	6.241	7.047	6.627	7.231	7.789
EA (eV)	1.678	2.516	3.203	0.602	0.126
Eg (eV)	4.563	4.531	3.424	6.629	7.663
η(eV)	2.2815	2.265	1.712	3.3145	3.8315
S $(eV)^{-1}$	0.219	0.441	0.584	0.151	0.130
χ(eV)	3.9595	4.781	4.915	3.9165	3.9575
μ (eV)	-3.9595	-4.781	-4.915	-3.9165	-3.9575
ω (eV)	3.436	5.045	7.055	2.314	2.044
$ε(eV)^{-1}$	0.291	0.198	0.141	0.432	0.489
ΔN	1.735	-0.566	-0.428	1.182	1.033
$ΔE_{(back\text{-}donation)}$(eV)	-0.570	0.489	0.608	-0.829	-0.958

Table 3. Quantum chemical parameters in aqueous medium at B3LYP/6–311 G++(d,p).

Indices	2-amino benzimidazole	2-methyl benzimidazol	2-mercapto benzimidazole	benzimidazole	benzotriazole
E_{HOMO} (eV)	-7.247	-7.047	-6.871	-7.231	-7.778
E_{LUMO} (eV)	-0.615	-0.516	-0.246	-0.602	-0.197
IP (eV)	7.247	7.047	6.871	7.231	7.778
EA (eV)	0.615	0.516	0.246	0.602	0.197
Eg (eV)	6.632	6.531	6.625	6.629	7.581
η(eV)	3.316	3.2655	3.3125	3.3145	3.7905
S $(eV)^{-1}$	0.151	0.153	0.151	0.151	0.132
χ(eV)	3.931	3.7815	3.5585	3.9165	3.9875
μ (eV)	-3.931	-3.7815	-3.5585	-3.9165	-3.9875
ω (eV)	2.330	2.190	1.911	2.314	2.097
$ε(eV)^{-1}$	0.429	0.457	0.523	0.432	0.477
ΔN	1.185	1.158	1.074	1.182	1.052
$ΔE_{(back\text{-}donation)}$(eV)	-0.829	-0.816	-0.828	-0.829	-0.948

Table 4. Quantum chemical parameters in aqueous medium at b2plypd3/aug-cc-pvdz.

Indices	2-amino benzimidazole	2-methyl benzimidazol	2-mercapto benzimidazole	benzimidazole	benzotriazole
E_{HOMO} (eV)	-5.767	-6.531	-4.151	-5.772	-6.431
E_{LUMO} (eV)	-0.365	-1.692	-0.689	-0.791	-1.427
IP (eV)	5.767	6.531	4.151	5.772	6.431
EA (eV)	0.365	1.692	0.689	0.791	1.427
Eg (eV)	5.402	4.839	3.462	4.981	5.004
η(eV)	2.701	2.4195	1.731	2.4905	2.502
S $(eV)^{-1}$	0.185	0.207	0.577701	0.401526	0.200
χ(eV)	3.066	4.112	2.42	3.2815	3.929
μ (eV)	-3.066	-4.112	-2.42	-3.2815	-3.929
ω (eV)	1.740	3.493	1.691623	2.161864	3.085
$\varepsilon(eV)^{-1}$	0.575	0.286	0.591148	0.462564	0.324
ΔN	0.354	0.179	1.322935	0.746537	0.210
$\Delta E_{(back\text{-}donation)}$(eV)	-0.675	-0.605	-0.43275	-0.62263	-0.626

the inhibitors and the metal surface. The $E_{Back\text{-}donation}$ suggests that charge transfer to a molecule, followed by a back-donation from the molecule, is energetically favored, when $\eta > 0$ and $E_{Back\text{-}donation} < 0$. Consequently, the following sequence is observed: 2-mercaptobenzimidazole > 2-methylbenzimidazol > benzimidazole > benzotriazole > 2-aminobenzimidazole, indicating that back donation is preferred for the 2-methylbenzimidazol, which is the most effective inhibitor.

Dipole moment: Another unique feature indicated in Tables 5 and 6 are the dipole moment in gas and aqueous phases. While prior research has not revealed a significant relationship between dipole moment and corrosion inhibition efficiency, the inhibitory efficiency shows that a large dipole moment indicates high corrosion inhibition potency [18, 31]. Several research revealed that decreasing the dipole moment value promoted corrosion.

Table 5. Dipole moments in gas phase and aqueous at B3LYP/6–311 G++(d,p).

Dipole moment (Debye)	2-amino benzimidazole	2-methyl benzimidazol	2-mercapto benzimidazole	benzimidazole	benzotriazole
Gas phase	3.555	3.272	3.855	3.482	3.398
Water	5.624	4.176	5.904	5.586	5.202

Table 6. Dipole moments in gas phase and aqueous at b2plypd3/aug-cc-pvdz.

Dipole moment (Debye)	2-amino benzimidazole	2-methyl benzimidazol	2-mercapto benzimidazole	benzimidazole	benzotriazole
Gas phase	4.708	3.580	5.034	3.642	4.251
Water	6.279	5.028	7.454	5.961	5.778

The dipole moment (μ) is a polarity measurement for a polar covalent bond. It is computed as the total of the atom charges and the distance between the two bound atoms [32]. Therefore, the total dipole moment only represents a molecule's global polarity. For a perfect nucleus, the vector sum of the individual bond dipole moments may be used to estimate the sum of the molecular dipole moments. However, a high dipole moment indicates a low bandgap and high softness, which increases the inhibition ability of the material as shown in Tables 5 and 6. The ranking of materials used for corrosion on this parameter is as follows: 2-mercaptobenzimidazole > 2-methylbenzimidazol > benzotriazole > 2-aminobenzimidazole.

Thermal properties: The significant thermodynamic parameters for the title compounds such as enthalpy (H), entropy (S), free energy (ΔG) and heat capacity (Cv) was estimated by DFT with the 6-311++G (d, p) basis set in various temperatures. Also, thermodynamic results derived from theoretical approaches are significant for comprehending chemical processes [17, 33]. The thermodynamic parameters are illustrated in Fig. 4. It was observed that entropy, heat capacity, and enthalpy increase as temperature rises. Whereas, free energy decreases with increasing temperatures.

Fukui function analysis: The selected inhibitors' local reactivity can be determined by measuring the Fukui indices of each of their atoms [34, 35]. The Fukui indices give more comprehensive information on the reactivity

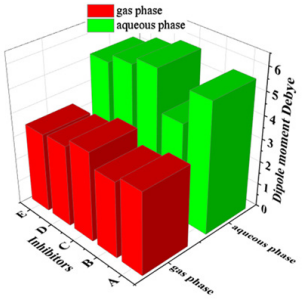

Fig. 3. Dipole moment variation among inhibitors in gas and aqueous phases.

of the compounds under investigation. In general, the greatest f^- signifies the site for electrophilic assault or when the inhibitor receives electrons, whereas the highest f^+ indicates the site for nucleophilic attack or when the inhibitor gives electrons [36]. Tables 7 to 16 shows how condensed Fukui indices are used to examine a molecule's local reactivity. The most reactive locations for nucleophilic assault are S (1), N (1,2), and C (8) atoms for 2-mercaptobenzimidazole, benzotriazole, and 2-methylbenzimidazol, respectively. suggesting a proclivity to transfer electrons to unoccupied molecular orbitals on the Fe surface to form a coordinating bond, whereas S (1) is the most reactive site for electrophilic attack for 2-mercaptobenzimidazole.

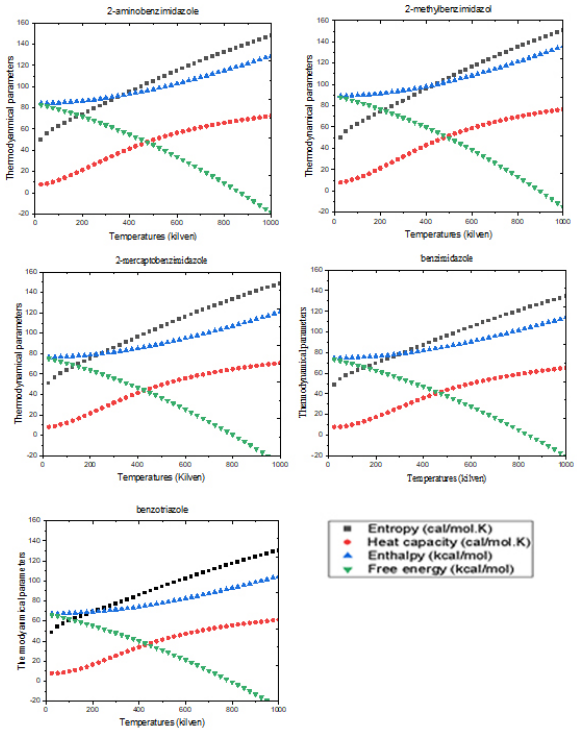

Fig. 4. Thermal properties of the title compounds.

Table 7. Fukui functions for 2-Aminobenzimidazole from NBO charges at 6-311++G (d, p).

Atoms	q(N)	q(N+1)	q(N-1)	F^+	F^-
N 1	-0.58996	-0.57746	-0.70082	0.0125	0.11086
N 2	-0.56464	-0.43287	-0.59576	0.13177	0.03112
N 3	-0.80844	-0.65574	-0.97046	0.1527	0.16202
C 4	0.12097	0.20784	0.07254	0.08687	0.04843
C 5	0.12258	0.18676	0.12569	0.06418	-0.00311
C 6	0.58267	0.63212	0.35004	0.04945	0.23263
C 7	-0.24503	-0.24094	-0.28288	0.00409	0.03785
C 8	-0.21101	-0.1509	-0.2324	0.06011	0.02139
C 9	-0.21949	-0.05182	-0.24441	0.16767	0.02492
C 10	-0.22075	-0.1808	-0.24233	0.03995	0.02158
H 11	0.40411	0.43501	0.30343	0.0309	0.10068
H 12	0.20626	0.24368	0.20166	0.03742	0.0046
H 13	0.21495	0.2504	0.19993	0.03545	0.01502
H 14	0.2037	0.23618	0.18807	0.03248	0.01563
H 15	0.20388	0.24095	0.1873	0.03707	0.01658
H 16	0.41046	0.43704	0.37064	0.02658	0.03982
H 17	0.38974	0.42055	0.26976	0.03081	0.11998

Table 8. Fukui functions for 2-Aminobenzimidazole from NBO charges at b2plypd3/aug-cc-pvdz.

Atoms	q(N)	q(N+1)	q(N-1)	F^+	F^-
N 1	-0.65084	-0.63871	-0.66604	0.01213	0.0152
N 2	-0.57658	-0.41275	-0.60406	0.16383	0.02748
N 3	-0.88981	-0.74979	-0.92594	0.14002	0.03613
C 4	0.12476	0.19473	0.13692	0.06997	-0.01216
C 5	0.11303	0.16018	0.05505	0.04715	0.05798
C 6	0.61687	0.66735	0.51041	0.05048	0.10646
C 7	-0.27686	-0.26631	-0.45859	0.01055	0.18173
C 8	-0.23964	-0.16453	-0.42067	0.07511	0.18103
C 9	-0.25480	-0.10256	-0.35573	0.15224	0.10093
C 10	-0.26021	-0.24602	-0.26334	0.01419	0.00313
H 11	0.44397	0.47818	0.41136	0.03421	0.03261
H 12	0.24321	0.28347	0.18780	0.04026	0.05541
H 13	0.25420	0.29196	0.19904	0.03776	0.05516
H 14	0.24262	0.28110	0.19023	0.03848	0.05239
H 15	0.24320	0.28476	0.19419	0.04156	0.04901
H 16	0.44413	0.47700	0.41606	0.03287	0.02807
H 17	0.42276	0.46194	0.39331	0.03918	0.02945

Table 9. Fukui functions for 2-methylbenzimidazole from NBO charges at 6-311++G (d, p).

Atoms	q(N)	q(N+1)	q(N-1)	F^+	F^-
N 1	-0.59416	-0.5855	-0.61686	0.00866	0.0227
N 2	-0.49208	-0.40284	-0.54799	0.08924	0.05591
N 3	0.11621	0.17472	0.12577	0.05851	-0.00956
C 4	0.09958	0.19598	0.06398	0.0964	0.0356
C 5	0.3993	0.5393	0.26091	0.14	0.13839
C 6	-0.27407	-0.23455	-0.41101	0.03952	0.13694
C 7	-0.22864	-0.13992	-0.37335	0.08872	0.14471
C 8	-0.73878	-0.76768	-0.71958	-0.0289	-0.0192
C 9	-0.24856	-0.05646	-0.34036	0.1921	0.0918
C 10	-0.26457	-0.25528	-0.27886	0.00929	0.01429
H 11	0.44651	0.47843	0.40532	0.03192	0.04119
H 12	0.2443	0.28551	0.19435	0.04121	0.04995
H 13	0.25389	0.29342	0.20455	0.03953	0.04934
H 14	0.27929	0.30582	0.24825	0.02653	0.03104
H 15	0.25516	0.29892	0.19668	0.04376	0.05848
H 16	0.25515	0.29892	0.19669	0.04377	0.05846
H 17	0.24553	0.28283	0.19395	0.0373	0.05158
H 18	0.24593	0.28839	0.19755	0.04246	0.04838

Table 10. Fukui functions for 2-methylbenzimidazole from NBO charges at b2plypd3/aug-cc-pvdz.

Atoms	q(N)	q(N+1)	q(N-1)	F^+	F^-
N 1	-0.60115	-0.61129	-0.62353	-0.01014	0.02238
N 2	-0.53398	-0.49499	-0.57186	0.03899	0.03788
N 3	0.13556	0.25379	0.16103	0.11823	-0.02547
C 4	0.11311	0.27059	0.07348	0.15748	0.03963
C 5	0.45637	0.61290	0.31785	0.15653	0.13852
C 6	-0.23872	-0.25220	-0.44002	-0.01348	0.20130
C 7	-0.18841	-0.16663	-0.39197	0.02178	0.20356
C 8	-0.59665	-0.62819	-0.58188	-0.03154	-0.01477
C 9	-0.20088	0.00325	-0.32246	0.20413	0.12158
C 10	-0.22189	-0.15808	-0.22284	0.06381	0.00095
H 11	0.41043	0.44382	0.38423	0.03339	0.02620
H 12	0.20493	0.24619	0.17103	0.04126	0.03390
H 13	0.21353	0.25420	0.17807	0.04067	0.03546
H 14	0.23079	0.25571	0.20842	0.02492	0.02237
H 15	0.20706	0.24835	0.16330	0.04129	0.04376
H 16	0.20705	0.24836	0.16327	0.04131	0.04378
H 17	0.20106	0.23322	0.16712	0.03216	0.03394
H 18	0.20177	0.24101	0.16678	0.03924	0.03499

Table 11. Fukui functions for 2-mercaptobenzimidazole from NBO charges at 6-311++G (d, p).

Atoms	q(N)	q(N+1)	q(N-1)	F^+	F^-
N 1	-0.21147	0.25286	-0.45750	0.46433	0.24603
N 2	-0.59253	-0.52023	-0.59812	0.07230	0.00559
N 3	-0.59253	-0.52023	-0.59812	0.07230	0.00559
C 4	0.13260	0.17550	0.12309	0.04290	0.00951
C 5	0.13260	0.17550	0.12309	0.0429	0.00951
C 6	-0.26392	-0.24545	-0.44032	0.01847	0.1764
C 7	-0.26392	-0.24545	-0.44032	0.01847	0.1764
C 8	0.21230	0.15003	0.12816	-0.06227	0.08414
C 9	-0.24813	-0.17228	-0.29930	0.07585	0.05117
C 10	-0.24813	-0.17228	-0.29930	0.07585	0.05117
H 11	0.46569	0.49203	0.44298	0.02634	0.02271
H 12	0.46569	0.49203	0.44298	0.02634	0.02271
H 13	0.25366	0.28419	0.21919	0.03053	0.03447
H 14	0.25366	0.28419	0.21919	0.03053	0.03447
H 15	0.25221	0.28481	0.21716	0.0326	0.03505
H 16	0.25221	0.28481	0.21716	0.0326	0.03505

Table 12. Fukui functions for 2-mercaptobenzimidazole from NBO charges at b2plypd3/aug-cc-pvdz.

Atoms	q(N)	q(N+1)	q(N-1)	F^+	F^-
N 1	-0.24311	0.27773	-0.46707	0.52084	0.22396
N 2	-0.62884	-0.54632	-0.64526	0.08252	0.01642
N 3	-0.62884	-0.54632	-0.64526	0.08252	0.01642
C 4	0.14342	0.1821	0.16007	0.03868	-0.01665
C 5	0.14342	0.1821	0.16007	0.03868	-0.01665
C 6	-0.26058	-0.24911	-0.42313	0.01147	0.16255
C 7	-0.26058	-0.24911	-0.42313	0.01147	0.16255
C 8	0.27843	0.17591	0.22111	-0.10252	0.05732
C 9	-0.2449	-0.172	-0.26422	0.0729	0.01932
C 10	-0.2449	-0.172	-0.26422	0.0729	0.01932
H 11	0.47007	0.49533	0.42685	0.02526	0.04322
H 12	0.47007	0.49533	0.42685	0.02526	0.04322
H 13	0.25263	0.28144	0.18454	0.02881	0.06809
H 14	0.25263	0.28144	0.18454	0.02881	0.06809
H 15	0.25054	0.28175	0.18413	0.03121	0.06641
H 16	0.25054	0.28175	0.18413	0.03121	0.06641

Table 13. Fukui functions for Benzimidazole from NBO charges at 6-311++G (d, p).

Atoms	q(N)	q(N+1)	q(N-1)	F^+	F^-
N 1	-0.55903	-0.49233	-0.60401	0.06670	0.04498
N 2	-0.48840	-0.43388	-0.52476	0.05452	0.03636
N 3	0.12026	0.25476	0.11523	0.13450	0.00503
C 4	0.10251	0.17231	0.09986	0.06980	0.00265
C 5	-0.23584	-0.16698	-0.23749	0.06886	0.00165
C 6	-0.18982	-0.16116	-0.20594	0.02866	0.01612
C 7	-0.20154	-0.16785	-0.22276	0.03369	0.02122
C 8	0.24262	0.31933	0.24088	0.07671	0.00174
C 9	-0.21938	0.00956	-0.23469	0.22894	0.01531
C 10	0.40740	0.44433	-0.04663	0.03693	0.45403
H 11	0.20727	0.24865	0.05318	0.04138	0.15409
H 12	0.21537	0.25723	0.19955	0.04186	0.01582
H 13	0.18983	0.23288	0.05203	0.04305	0.13780
H 14	0.20400	0.24561	0.14150	0.04161	0.06250
H 15	0.20476	0.23753	0.17404	0.03277	0.03072

Using natural bonding orbitals (NBOs), it was performed in b2plypd3/aug-cc-pvdz basis set for all identified molecules. It is assumed that the more negative the atomic charges of the adsorbed center, the more

Table 14. Fukui functions for Benzimidazole from NBO charges at b2plypd3/aug-cc-pvdz.

Atoms	q(N)	q(N+1)	q(N-1)	F^+	F^-
N 1	-0.62810	-0.63317	-0.65267	-0.00507	0.02457
N 2	-0.51148	-0.47351	-0.56252	0.03797	0.05104
N 3	0.12383	0.23834	0.13625	0.11451	-0.01242
C 4	0.09846	0.26597	0.07257	0.16751	0.02589
C 5	-0.27166	-0.28196	-0.44297	-0.01030	0.17131
C 6	-0.22090	-0.20116	-0.39730	0.01974	0.17640
C 7	-0.24100	-0.02990	-0.36080	0.21110	0.11980
C 8	0.23895	0.39380	0.01868	0.15485	0.22027
C 9	-0.26365	-0.20402	-0.28470	0.05963	0.02105
C 10	0.45467	0.49021	0.42548	0.03554	0.02919
H 11	0.24439	0.28894	0.21068	0.04455	0.03371
H 12	0.25415	0.29819	0.21901	0.04404	0.03514
H 13	0.23281	0.27813	0.20104	0.04532	0.03177
H 14	0.24453	0.28180	0.20800	0.03727	0.03653
H 15	0.24501	0.28833	0.20924	0.04332	0.03577

Table 15. Fukui functions for Benzotriazole from NBO charges at 6-311++G (d, p).

Atoms	q(N)	q(N+1)	q(N-1)	F^+	F^-
N 1	-0.24214	-0.11250	-0.35568	0.12964	0.11354
N 2	-0.03696	0.02232	-0.20572	0.05928	0.16876
N 3	0.07023	0.04386	0.06581	-0.02637	0.00442
C 4	0.11494	0.11329	0.12380	-0.00165	-0.00886
C 5	-0.17605	0.00586	-0.34877	0.18191	0.17272
C 6	-0.23122	-0.02342	-0.38865	0.20780	0.15743
C 7	-0.21743	-0.08827	-0.24576	0.12916	0.02833
C 8	-0.18287	-0.17423	-0.30127	0.00864	0.11840
C 9	0.22161	0.25652	0.18384	0.03491	0.03777
C 10	0.21330	0.24776	0.17596	0.03446	0.03734
H 11	0.20933	0.24776	0.17208	0.03843	0.03725
H 12	0.20813	0.25086	0.17123	0.04273	0.03690
H 13	-0.36095	-0.23681	-0.42099	0.12414	0.06004
H 14	0.41009	0.44700	0.37415	0.03691	0.03594

Table 16. Fukui functions for Benzotriazole from NBO charges at b2plypd3/aug-cc-pvdz.

Atoms	q(N)	q(N+1)	q(N-1)	F^+	F^-
N 1	-0.24373	-0.14314	-0.41027	0.10059	0.16654
N 2	-0.02878	0.04462	-0.18979	0.07340	0.16101
N 3	0.06014	0.04226	0.08845	-0.01788	-0.02831
C 4	0.12740	0.13391	0.14712	0.00651	-0.01972
C 5	-0.19706	0.01341	-0.34087	0.21047	0.14381
C 6	-0.26492	-0.03698	-0.38601	0.22794	0.12109
C 7	-0.25609	-0.09698	-0.24802	0.15911	-0.00807
C 8	-0.21005	-0.19179	-0.30920	0.01826	0.09915
C 9	0.25322	0.27386	0.19397	0.02064	0.05925
C 10	0.24431	0.26268	0.18351	0.01837	0.06080
H 11	0.24151	0.26397	0.18196	0.02246	0.05955
H 12	0.24089	0.26552	0.17916	0.02463	0.06173
H 13	-0.41643	-0.31431	-0.49396	0.10212	0.07753
H 14	0.44960	0.48297	0.40395	0.03337	0.04565

readily the atom gives its electrons to the metal/metal oxide's empty orbital. Table 8, 10, 12, 14 and 16 shows that nitrogen atoms have negative charge centers that might give electrons to the iron surface to establish a coordinate-type connection, the highest negative values are bolded in the Tables 8, 10, 12, 14 and 16.

Monte Carlo stimulation: The Monte Carlo simulation is often used to investigate the interaction between a

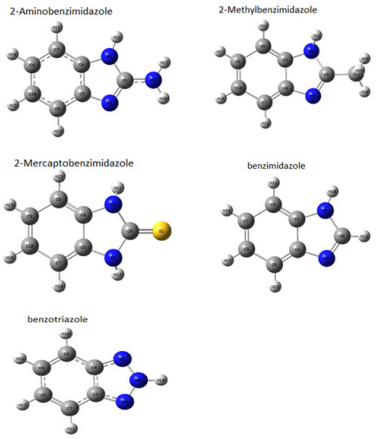

Fig. 5. Optimized molecule structures based on DFT at 6-311++G(d,p) basis set.

molecule inhibitor and a metal surface [37].

This method can illustrate one of the most important aspects of the corrosion problem: the adsorption phenomena. The most stable adsorption sites are found on low-energy metal surfaces. In molecular dynamics simulations done with the adsorption locator and the Forcite code, to determine a feasible position for the interaction between the inhibitor and the Fe surface provided in Material Studio 7.0 software [38].

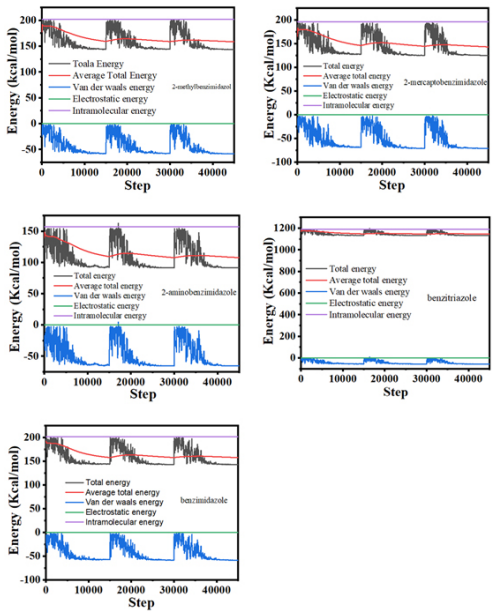

Fig. 6. Typical energy based on Monte Carlo stimulation of selected molecules.

Using a Monte Carlo simulation, Fig. 6 depicts the most stable low-energy energy adsorption arrangement of inhibitors in the Fe (110) system of a typical energy (total energy, average total energy, van der Waals energy, electrostatic energy, and intermolecular energy. These properties, which include structural, conformational, vibration and state equations, cohesive energy, and interaction energy for a wide range of organic metal molecules, metal oxides, and metal halides, make use of a variety of solid properties such as cell unit structure, lattice energy, and even polymers [6]. The initial phase in this computer analysis is to optimize the shape of the inhibitor molecule, which will adsorb next on the iron surface with the least amount of energy [39]. The Forcite computation was completed with excellent estimation accuracy utilizing the COMPASS forcefield for this reason [40].

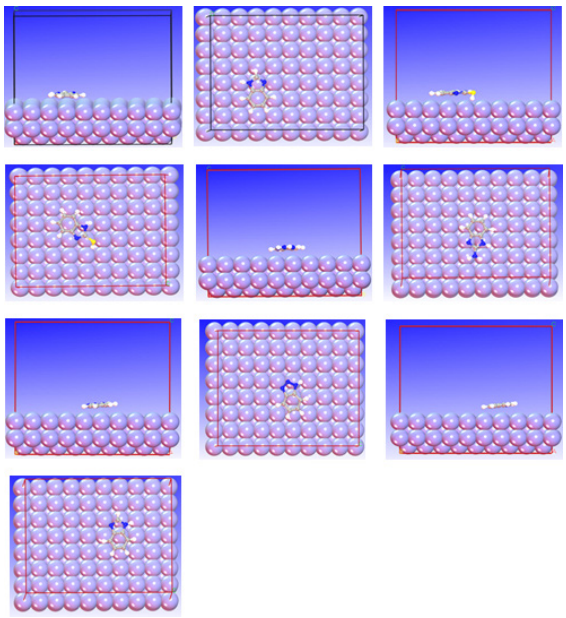

Fig. 7. Top and side views of the most stable low energy configuration for the adsorption for all selected molecules in this study.

As a result of using the Monte Carlo method, several properties were obtained such as total adsorption e, solid adsorption and deformation energies as shown in Table 17. The adsorption energy is the energy released during the adsorption process. The adsorption energy, is ascribed to the energy produced by the flexible adsorption compounds placed on the substrate.

Table 17. The outputs and descriptors calculated by the Monte Carlo simulation for adsorption on Fe (110) (in kcal mol^{-1}) and experimental inhibition efficiency [6].

Inhibitors	Total energy	Adsorption energy	Rigid adsorption energy	Deformation energy	dE_{ad}/dN_i	% IE
2-meythyl benzimidazole MBIH	143.58452186	-58.65350403	-58.6535040	-3.764995×10^{-9}	-58.6535040	80
2-mercapto benzimidazole 2-CH3-BI	124.73065649	-71.76095653	-71.7609565	-1.234270×10^{-9}	-71.7609565	96.39
2-amino benzimidazole (2-ABI)	95.84806853	-43.17668955	-43.1766895	-7.105427×10^{-13}	-43.1766895	42.45
Benzotriazole (BTA)	1.134599e+003	-53.51120229	-53.5112022	-1.032276×10^{-10}	-53.5112022	-
Benzimidazole (BIM)	145.57694973	-56.04159478	-56.0415947	7.958079×10^{-3}	-56.0415947	56.21

The adsorption energies of the inhibitors are estimated by summing energy of solid adsorption and adsorbent structural deformation, as shown in Table 17. Higher negative adsorption energy values, as displayed in Fig. 7, indicate that the association between a metal and inhibitor molecules is more stable and stronger.

CONCLUSIONS

The present study on the inhibition efficiency 2-aminobenzimidazole, 2-methylbenzimidazol, 2-mercaptobenzimidazole and benzimidazole in combination with benzotriazole has lead us 2-methylbenzimidazol was the most efficient inhibitor for iron metal in gas and solvent medium. The calculation of chemical reactivity parameters shows that the inhibition efficiency follows the-order 2-methylbenzimidazol > benzotriazole > 2-aminobenzimidazole > 2-mercapto-benzimidazole > benzimidazole.

Our calculations using Fukui function predicted the nucleophilic and electrophilic attacking sites of the inhibitors. The results of quantum chemical computations and experimental investigations were in a good agreement.

REFERENCES

1. Wang, N., Xiong, D., Deng, Y., Shi, Y., Wang, K. (2015) Mechanically robust superhydrophobic steel surface with anti-icing, UV-durability, and corrosion resistance properties. *ACS Appl. Mater. Interfaces*, **7**, 6260-6272. https://doi.org/10.1021/acsami.5b00558
2. Qadr, H.M. (2021) A molecular dynamics study of temperature dependence of the primary state of cascade damage processes. *Russ. J. Non-Ferr.*, **62**, 561-567. https://doi.org/10.3103/S1067821221050096
3. Balamurugan, A., Rajeswari, S., Balossier, G., Rebelo, A.H.S., Ferreira, J.M.F. (2008) Corrosion aspects of metallic implants - An overview. *Corros. Mater.*, **59**, 855-869. https://doi.org/10.1002/maco.200804173
4. Qadr, H.M. (2020) Effect of ion irradiation on the mechanical properties of high and low copper. *At. Indones.*, **46**, 47-51. https://doi.org/10.17146/aij.2020.923
5. Ahamed, M.R., Narren, S.F., Sadiq, A.S. (2013) Synthesis of 2-mercaptobenzimidazole and some of its derivatives. *ANJS.*, **16**, 77-83. https://doi.org/10.22401/JNUS.16.2.11
6. Liu, L., Lu, S., Wu, Y.Q., Xie, J.Y., Xing, J. (2020) Corrosion inhibition behavior of four benzimidazole derivatives and benzotriazole on copper surface. *Anti-Corros. Methods Mater.*, **67**, 565-574. https://doi.org/10.1108/ACMM-12-2019-2235
7. Altaf, M., Yamin, N., Muhammad, G., Raza, M.A., Shahid, M., *et al*. (2021) Electroanalytical techniques for the remediation of heavy metals from wastewater. *Water Pollution and Remediation: Heavy Metals*, 471-511. https://doi.org/10.1007/978-3-030-52421-0_14
8. Gupta, V.K., Ali, I. (2013) *Environmental water: advances in treatment, remediation and recycling*, 2nd Ed., Elsevier, Oxford, UK. https://doi.org/10.1016/B978-0-444-59399-3.00008-8
9. Qadr, H.M. (2021) Pressure effects on stopping power of alpha particles in argon gas. *Phys. Part. Nucl.*, **18**, 185-189. https://doi.org/10.1134/S1547477121020151
10. Tan, Y., Leonhard, M., Moser, D., Ma, S., Schneider-Stickler, B. (2019) Antibiofilm efficacy of curcumin in combination with 2-aminobenzimidazole against single-and mixed-species biofilms of Candida albicans and Staphylococcus aureus. *Colloids Surf. B: Biointerfaces.*, **174**, 28-34. https://doi.org/10.1016/j.colsurfb.2018.10.079
11. Song, D., Ma, S. (2016) Recent development of benzimidazole-containing antibacterial agents. *Chem.Med.Chem.*, **11**, 646-659. https://doi.org/10.1002/cmdc.201600041
12. Briguglio, I., Piras, S., Corona, P., Gavini, E., Nieddu, M., *et al*. (2015) Benzotriazole: An overview on its versatile biological behavior. *Eur. J. Med. Chem.*, **97**, 612-648. https://doi.org/10.1016/j.ejmech.2014.09.089
13. Pustuła, K., Płonka, A., Makowski, M. (2018) Thermal decomposition of oxetan-2-one molecule in the light of DFT and CASPT2 modelling. *Comput. Theor. Chem.*, **1140**, 98-103. https://doi.org/10.1016/j.comptc.2018.07.020
14. Frisch, A. (2009) Gaussian 09W Reference. *Wallingford, USA, 25 p*, **470**.
15. Cammi, R., Mennucci, B. (1999) Linear response theory for the polarizable continuum model. *J. Chem. Phys.*, **110**, 9877-9886. https://doi.org/10.1063/1.478861
16. Hussein, Y.T., Azeez, Y.H. (2021) DFT analysis and in silico exploration of drug-likeness, toxicity prediction, bioactivity score, and chemical reactivity properties of the urolithins. *J. Biomol. Struct. Dyn.*, 1-10. https://doi.org/10.1080/07391102.2021.2017350
17. Qadr, H.M., Mamand, D.M. (2021) Molecular structure and density functional theory investigation corrosion inhibitors of some oxadiazoles. *J. Bio-Tribo-Corros.*, **7**, 140. https://doi.org/10.1007/s40735-021-00566-9
18. Mamand, D.M., Rasul, H.H., Omer, P.K., Qadr, H.M. (2022) Theoretical and experimental investigation on ADT organic semiconductor in different solvents. *Condens. Matter Interphases.*, **24**, 227-242. https://doi.org/10.17308/kcmf.2022.24/9263
19. Outirite, M., Lagrenée, M., Lebrini, M., Traisnel, M., Jama, C., *et al*. (2010) ac impedance, X-ray photoelectron spectroscopy and density functional theory studies of 3, 5-bis (n-pyridyl)-1, 2, 4-oxadiazoles as efficient corrosion inhibitors

for carbon steel surface in hydrochloric acid solution. *Electrochim. Acta.*, **55**, 1670-1681. https://doi.org/10.1016/j.electacta.2009.10.048
20. Mamand, D.M., Anwer, T.M.K., Qadr, H.M. (2022) Theoretical investigation on corrosion inhibition effect of oxadiazole: DFT calculations. *Oxid. Commun.*, **45**, 600-627.
21. Ju, H., Ding, L., Sun, C., Chen, J.-j. (2015) Quantum chemical study on the corrosion inhibition of some oxadiazoles. *Adv. Mater. Sci. Eng.*, **2015**. https://doi.org/10.1155/2015/519606
22. Demissie, E.G., Kassa, S.B., Woyessa, G.W. (2014) Quantum chemical study on corrosion inhibition efficiency of 4-amino-5-mercapto-1, 2, 4-triazole derivatives for copper in HCl solution. *Int. J. Sci. Eng. Res.*, **5**, 304. https://doi.org/10.14299/ijser.2014.06.001
23. Mamand, D. (2019) Determination the band gap energy of poly benzimidazo-benzophenanthroline and comparison between HF and DFT for three different basis sets. *J. Phys. Chem. Funct. Mater.*, **2**, 32-36.
24. Zheng, X., Zhang, S., Gong, M., Li, W. (2014) Experimental and theoretical study on the corrosion inhibition of mild steel by 1-octyl-3-methylimidazolium L-prolinate in sulfuric acid solution. *Ind. Eng. Chem. Res.*, **53**, 16349-16358. https://doi.org/10.1021/ie502578q
25. Djenane, M., Chafaa, S., Chafai, N., Kerkour, R., Hellal, A. (2019) Synthesis, spectral properties and corrosion inhibition efficiency of new ethyl hydrogen [(methoxyphenyl)(methylamino) methyl] phosphonate derivatives: Experimental and theoretical investigation. *J. Mol. Struct.*, **1175**, 398-413. https://doi.org/10.1016/j.molstruc.2018.07.087
26. Chen, X., Chen, Y., Cui, J., Li, Y., Liang, Y., *et al*. (2021) Molecular dynamics simulation and DFT calculation of "green" scale and corrosion inhibitor. *Comput. Mater. Sci.*, **188**, 110229. https://doi.org/10.1016/j.commatsci.2020.110229
27. Singh, P., Srivastava, V., Quraishi, M.A. (2016) Novel quinoline derivatives as green corrosion inhibitors for mild steel in acidic medium: electrochemical, SEM, AFM, and XPS studies. *J. Mol. Liq.*, **216**, 164-173. https://doi.org/10.1016/j.molliq.2015.12.086
28. Kaya, S., Kaya, C., Islam, N. (2016) The nucleophilicity equalization principle and new algorithms for the evaluation of molecular nucleophilicity. *Comput. Theor. Chem.*, **1080**, 72-78. https://doi.org/10.1016/j.comptc.2016.02.006
29. Khaled, K.F. (2011) Experimental and computational investigations of corrosion and corrosion inhibition of iron in acid solutions. *J. Appl. Electrochem.*, **41**, 277-287. https://doi.org/10.1007/s10800-010-0235-2
30. Goulart, C.M., Esteves-Souza, A., Martinez-Huitle, C.A., Rodrigues, C.J.F., Maciel, M.A.M., *et al*. (2013) Experimental and theoretical evaluation of semicarbazones and thiosemicarbazones as organic corrosion inhibitors. *Corros. Sci.*, **67**, 281-291. https://doi.org/10.1016/j.corsci.2012.10.029
31. Qadr, H.M., Mamand, D. (2022) A Review on DPA for computing radiation damage simulation. *J. Phys. Chem. Funct. Mater.*, **5**, 30-36. https://doi.org/10.54565/jphcfum.1027393
32. Mamand, D. (2019) Theoretical calculations and spectroscopic analysis of gaussian computational examination-NMR, FTIR, UV-Visible, MEP on 2, 4, 6-Nitrophenol. *J. Phys. Chem. Funct. Mater.*, **2**, 77-86.
33. El Faydy, M., Galai, M., El Assyry, A., Tazouti, A., Touir, R., *et al*. (2016) Experimental investigation on the corrosion inhibition of carbon steel by 5-(chloromethyl)-8-quinolinol hydrochloride in hydrochloric acid solution. *J. Mol. Liq.*, **219**, 396-404. https://doi.org/10.1016/j.molliq.2016.03.056
34. Hadisaputra, S., Purwoko, A.A., Savalas, L.R.T., Prasetyo, N., Yuanita, E., *et al*. (2020) Quantum chemical and Monte Carlo simulation studies on inhibition performance of caffeine and its derivatives against corrosion of copper. *Coatings.*, **10**, 1086. https://doi.org/10.3390/coatings10111086
35. Erdoğan, Ş., Safi, Z.S., Kaya, S., Işın, D.Ö., Guo, L., *et al*. (2017) A computational study on corrosion inhibition performances of novel quinoline derivatives against the corrosion of iron. *J. Mol. Struct.*, **1134**, 751-761. https://doi.org/10.1016/j.molstruc.2017.01.037
36. Frenkel, D., Smit, B., Ratner, M.A. (1996) *Understanding molecular simulation: From algorithms to applications*, Academic press San Diego.
37. Mamand, D.M., Qadr, H.M. (2021) Comprehensive spectroscopic and optoelectronic properties of bbl organic semiconductor. *Prot. Met. Phys. Chem. Surf.*, **57**, 943-953. https://doi.org/10.1134/S207020512105018X
38. Guo, L., Zhu, S., Zhang, S. (2015) Experimental and theoretical studies of benzalkonium chloride as an inhibitor for carbon steel corrosion in sulfuric acid. *J. Ind. Eng. Chem.*, **24**, 174-180. https://doi.org/10.1016/j.jiec.2014.09.026
39. Mamand, D.M., Anwer, T.M.K., Qadr, H.M., Mussa, C.H. (2022) Investigation of spectroscopic and optoelectronic properties of phthalocyanine molecules. *Russ. J. Gen. Chem.*, **92**, 1827-1838. https://doi.org/10.1134/S1070363222090249
40. Mamand, D.M., Qadr, H.M. (2022) Density functional theory and computational simulation of the molecular structure on corrosion of carbon steel in acidic media of some amino acids. *Russ. J. Phys. Chem. A.*, **96**, 2155-2165. https://doi.org/10.1134/S0036024422100193